JOURNAL OF GEOPHYSICAL RESEARCH, VOL. 100, NO. B7, PAGES 12,487–12,495, JULY 10, 1995

Shallow and peripheral volcanic sources of inflation revealed by modeling two-color geodimeter and leveling data from Long Valley caldera, California, 1988–1992

John Langbein,[1] Daniel Dzurisin,[2] Grant Marshall,[1] Ross Stein,[1] and John Rundle[3]

Abstract. We refined the model for inflation of the Long Valley caldera near Mammoth Lakes, California, by combining both geodetic measurements of baseline length and elevation changes. Baseline length changes measured using a two-color geodimeter with submillimeter precision revealed that the resurgent dome started to reinflate in late 1989. Measurements between late 1989 and mid-1992 revealed nearly 13 cm of extension across the resurgent dome. Geodetic leveling surveys with approximately 2-mm precision made in late 1988 and in mid-1992 revealed a maximum of about 8 cm of uplift of the resurgent dome. Two ellipsoidal sources satisfy both the leveling and two-color measurements, whereas spherical point sources could not. The model's primary inflation source is located 5.5 km beneath the resurgent dome with the two horizontal axes being nearly equal in size and the vertical axis being 4 times the length of the horizontal axes. A second ellipsoidal source was added to improve the fit to the two-color measurements. This secondary source is located at a depth between 10 and 20 km beneath the south moat of the caldera and has the geometry of an elongated ellipsoid or pipe that dips down to the northeast. In addition, the leveling data suggest dike intrusion beneath Mammoth Mountain during the 1988–1992 interval, which is likely associated with an intense swarm of small earthquakes during the summer of 1989 at that location. Our analysis shows the dike intrusion to be the shallowest of the three sources with a depth range of 1–3 km below the surface to the top of the intrusion.

Introduction

In the past 15 years the Long Valley caldera, located east of the Sierra Nevada range in California, has had two episodes of rapid inflation without any eruption or deflation between episodes. The first episode started after 1976 (most likely after mid-1979) and continued into the 1980s. Evidence presented by *Langbein* [1989] and *Savage* [1988] showed that the rapid inflation measured in the first half of the decade slowed such that the strain rates approached background levels of the order of a few parts in 10^7 per year by 1988. *Langbein et al.* [1993a] established and *Dixon et al.* [1993] confirmed that the second round of inflation started in October 1989 and continues into 1995, and they argued that the second episode was driven primarily by a magmatic source rather than a regional tectonic source. This conclusion was based on the fact that the inflation preceded the renewal of seismicity and that the geodetic moment associated with the inflation is more than a factor of 10 greater than the seismic moment release within the caldera. This may also be true for the first episode of inflation but cannot be verified because frequent geodetic observations were lacking until mid-1983. Models used by previous studies, for example, *Langbein et al.* [1993a], all have in common a point source [*Mogi*, 1958] under the resurgent dome. With the addition of high-precision trilateration data, additional sources of deformation were needed to adequately model the observations. For the second episode of inflation, *Langbein et al.* [1993a] found that slip on one of the medial graben faults within the resurgent dome was a secondary source of deformation. The first episode was more complicated, requiring fault slip in the south moat plus a weak source of inflation near the southwest border of the resurgent dome.

With the additional leveling data [*Yamashita et al.*, 1992] that span the caldera and cover the period of the second inflation (1988–1992) it is our purpose to refine the models presented earlier. We use both the vertical displacements measured by leveling and the horizontal displacements measured using the two-color geodimeter network. We find that although two sources of inflation are required to model the data, these sources are nonspherical pressure sources, and we modeled these sources with ellipsoidal inclusions described by *Davis* [1986]. Significantly, we find the source beneath the resurgent dome to be at 5.5 km depth, which is 2–3 km shallower than found previously. Although poorly constrained, the second source is located either beneath the south moat or farther south at a depth in excess of 10 km. From the leveling data we can make additional inferences about the hypothesized dike injection beneath Mammoth Mountain in mid-1989 [*Hill et al.*, 1990; *Langbein et al.*, 1993a].

[1]U.S. Geological Survey, Menlo Park, California.
[2]U.S. Geological Survey, Vancouver, Washington.
[3]Cooperative Institute for Research in Environmental Science, Univ. of Colorado, Boulder.

Paper number 95JB01052.
0148-0227/95/95JB-01052$05.00

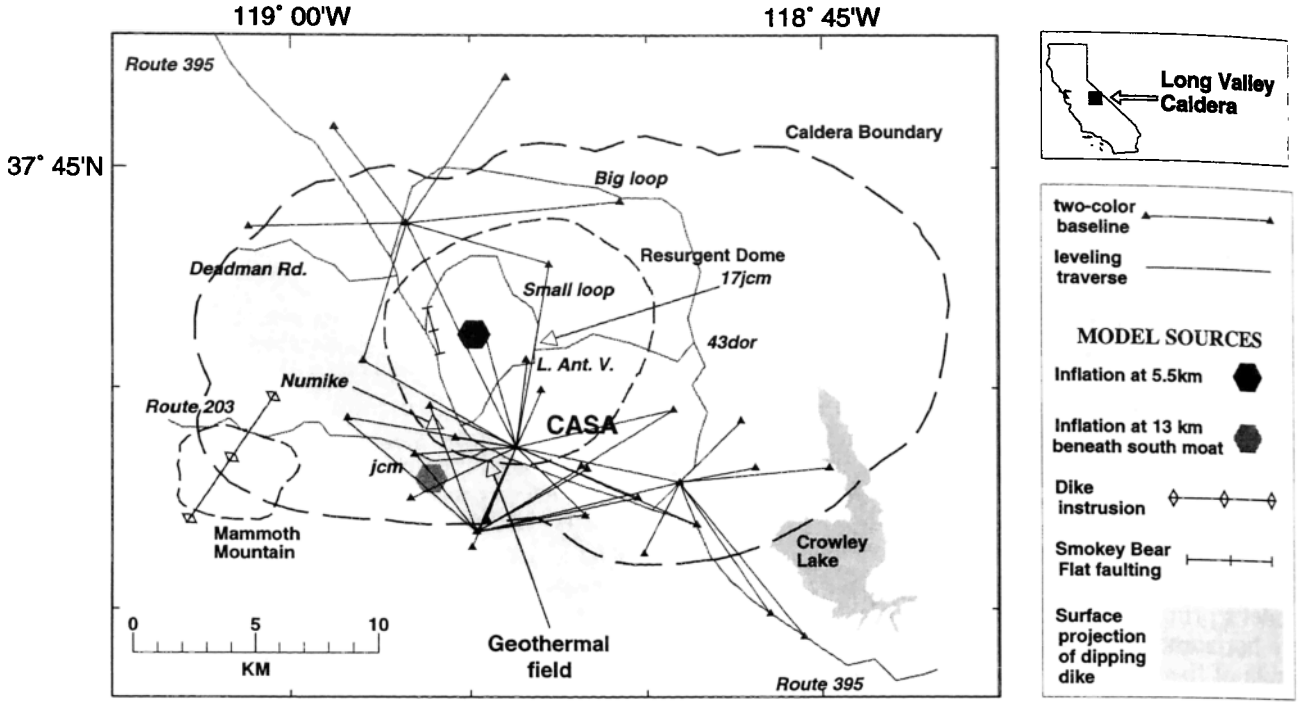

Figure 1. Map showing the location of the leveling traverses, the baselines measured using a two-color geodimeter, and the sources used in modeling the data for the period between late 1988 and mid-1992. The location of the caldera boundary and resurgent dome is from *Bailey* [1989]. The locations of the leveling traverses are shown with heavy grey lines, and the baselines are shown with thin solid lines. Only a few of the trilateration and leveling monuments are identified. The traverses are identified by their location: Route 395, Route 203, Deadman Road, Little Antelope Valley (L. Ant. V.), big loop, and small loop. The inflation source beneath the resurgent dome is common to all models and is identified with a solid hexagon at 37.6869° and 118.9150°. The other hexagon at 37.6325° and 118.9353° in the south moat represents a deeper inflation source that is used in some of the models discussed in the text. A dike that dips to the northeast is another possible model to describe part of the deformation. In addition, intrusion of a dike between 2 and 12 km beneath Mammoth Mountain and normal faulting in Smokey Bear flat are used to model the data.

Data

Complete leveling of the Long Valley caldera occurred in 1983, 1984, 1985, 1986, 1988, and 1992. Since we are most concerned with the deformation between late 1989 and the present, we limit the discussion to the 1988–1992 epoch. The map in Figure 1 shows the location of the leveling traverses measured in this epoch. Since the monument spacing is irregular, we achieve a more regular spatial sampling by eliminating some of the monuments. To minimize the effect of the statistical covariance in modeling leveling data, we model section or bench mark to bench mark differences rather than cumulative elevation differences [*Arnadottir et al.*, 1992]. We assume the standard error in leveling is normally distributed and accumulated as $\alpha L^{1/2}$, where L is the section length and $\alpha = 2.8$ mm/km$^{1/2}$ for change in elevation. The term α used here is larger than that specified for the first-order, second-class leveling done in 1988 and 1992, and α was computed on the basis of using misclosures of the four loops (Figure 1) measured in both surveys. The profiles of uplift along the seven traverses spanning the caldera are shown in Figure 2.

The data for the two-color geodimeter network were described most recently by *Langbein et al.* [1993a] for the interval between mid-1983 and the end of 1991. We have continued these measurements to the present. The line lengths in this geodetic network are measured from several times weekly to once yearly. Frequently measured lines share the central monument CASA (Figure 1) as a common endpoint. There are 41 baselines with measurements that span the 1988–1992 interval of the leveling, and their locations are shown in Figure 1. To extract the displacement and its error for each of these baselines during the 1988–1992 interval, we use the method employed by *Langbein et al.* [1987] in which a function of linear splines is fit with time to the displacement time series for each baseline. This has the advantage of averaging the data for the period of about a month and minimizes the influence of outliers. This analysis yields the displacement and standard error of each baseline for the epoch that spans the leveling. The linear spline technique is used in preference to simply fitting a single rate of extension for the period 1988–1992, because inspection of the data shows that the rate is not constant.

Although leveling data give a spatial sense to uplift, the signal-to-noise ratio of the two-color data vastly exceeds that of the leveling data (Table 1). The better signal-to-noise ratio of the two-color data is apparent when comparing the standard errors of the two-color measurements which range between 0.3 and 2.0 mm to those of the leveling which range between 2.5 and 4.5 mm. To accommodate the difference in noise level, we have chosen to downweight the two-color

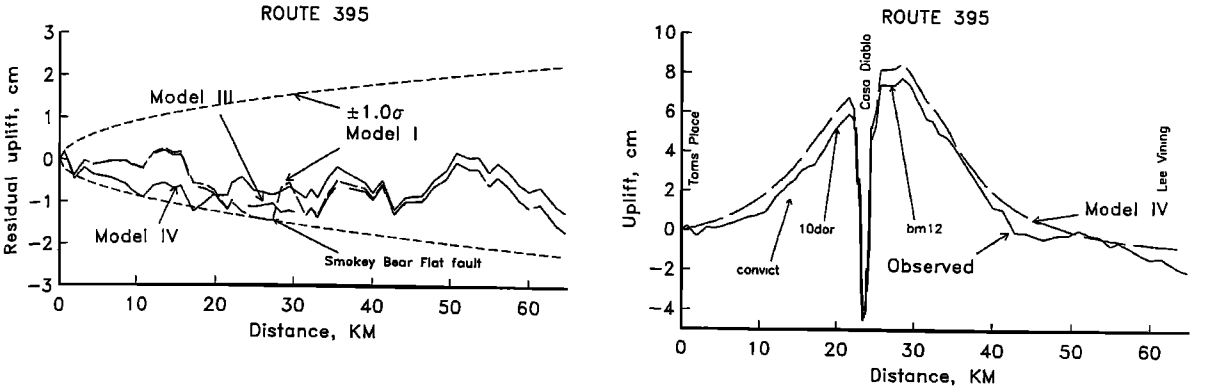

Figure 2a. Plots of uplift along surveyed leveling traverses in the Long Valley region for the interval between 1988 and 1992. Traverses are identified on each plot and are located on the map in Figure 1. The uplift profile is shown along Route 395 from Toms Place south of the caldera to Lee Vining just north of Mono Lake. In addition, the residual uplift is shown after removing the uplift produced by models I, III, and IV.

data when using the least squares method to fit the model to both sets of data. Justification for the increase of the error in two-color measurements comes from the fact that the formal standard error of 0.3–2.0 mm accounts for only the random error component due to the two-color technique [*Langbein*, 1989] but does not account for any time-dependent component to the noise [*Langbein et al.*, 1993b] due to the local motion of geodetic monuments [*Wyatt*, 1982] which we

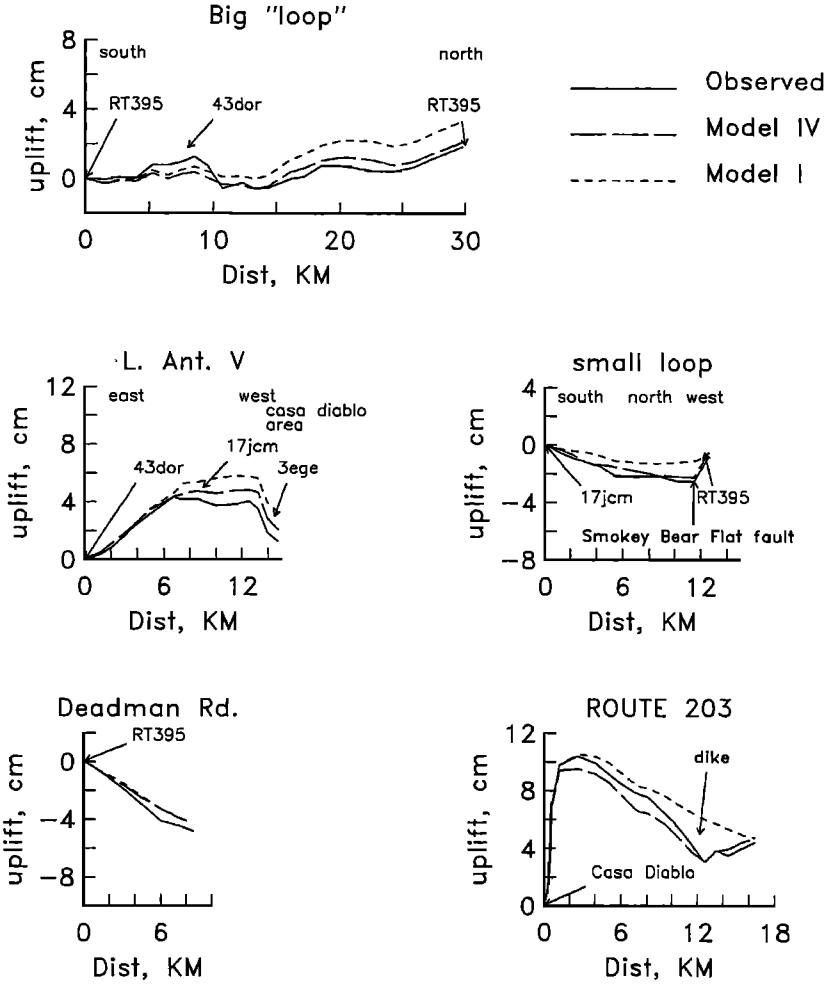

Figure 2b. The observed uplift profile and predicted uplift profiles from models I and IV for the remaining five traverses in the caldera. The line along Route 203 shows an inflection 13 km from Casa Diablo, which has been modeled as dike intrusion beneath Mammoth Mountain.

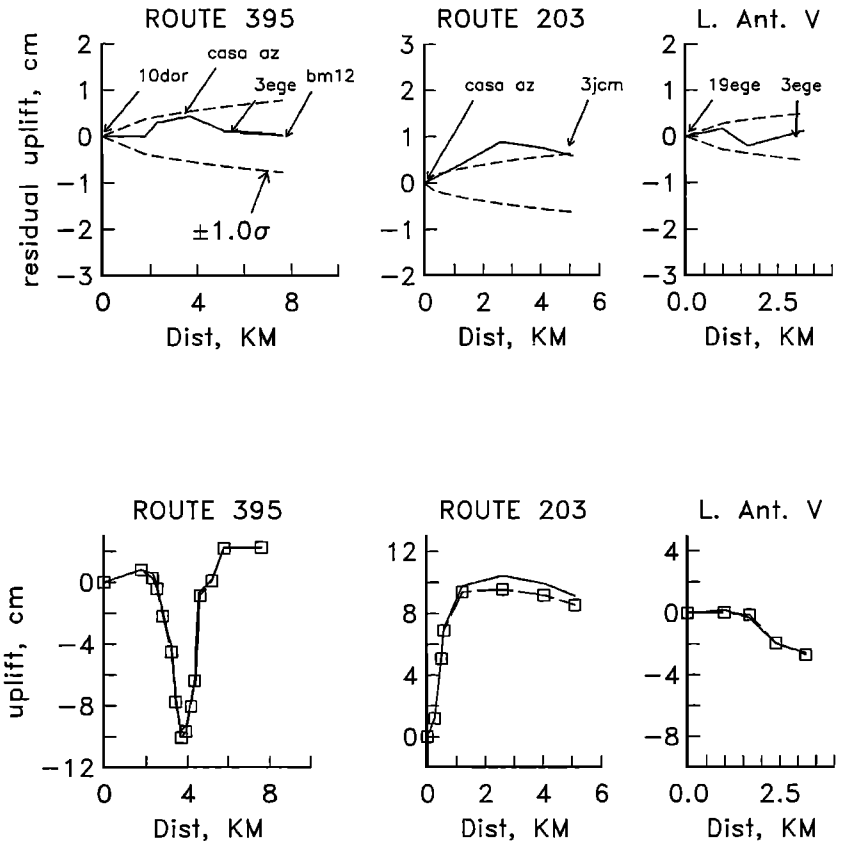

Figure 2c. The observed collapse, predicted collapse, and the residual vertical displacements of the area around the geothermal power plant near Casa AZ. The predicted collapse is calculated using a horizontal tensile fracture at 200 m depth.

believe could be of the order of 1–2 mm over this 4-year period. In absence of actual estimates of the size of the local motion of each monument, we have chosen to downweight the two-color data by a factor of 5 to account for the time-dependent component of noise in the data. In addition, downweighting the two-color data gives the leveling data more influence in the modeling. Adding an estimate of time-dependent noise to the leveling data is not necessary because its random component in excess of 3 mm exceeds the time-dependent component.

Both the leveling and the two-color data are a result of both long- and short-wavelength deformation. The deformation causing the uplift and the extension is most likely due to inflation of the resurgent dome, the details of which we are attempting to uncover. In addition, the leveling data also show subsidence concentrated within 1 km of the Casa Diablo Geothermal power plant. The short-wavelength subsidence is nearly equal and opposite in sense to the broad scale uplift of the dome and may affect the central site CASA that is common to many of the two-color measurements (Figure 1).

Modeling

We employ a grid search algorithm that specifies the location and geometry of a set of N sources to compute the influence of a unit of displacement from each source on the length of each baseline and on the relative uplift of each section, known as the A matrix. Using least squares to minimize the misfit between the observations and the calculated displacements, the magnitude of each source x is estimated. After changing one of the parameters that specifies the location or geometry of one source a new set of A matrices is computed, and x is determined again by least squares. This process is repeated by allowing a large set of source geometries and locations to change. A list is created of source locations and values of χ^2, the summation of the squares of the difference between the observed and predicted displacements normalized by the a priori data error, with the smallest χ^2 selected. In addition, the sensitivity of each parameter that specifies location, geometry, and size can be assessed graphically in terms of its effect on the model fit.

Table 1. Signal-to-Noise Ratios of the Data

Data Set	Number of Baselines/Sections	Signal-to-Noise Ratio
Two color	41	56.2
All leveling	124	4.8
Leveling near Casa Diablo Geothermal power plant	18	11.7
Leveling in remainder of caldera and its surroundings	106	1.9

Table 2. Models of Deformation

Model	CASA Displacement		χ^2			Time-Dependent Model Misfit Ratio, mm/mm
	West, mm	South, mm	Leveling, $(mm/mm)^2$	Two-color, $(mm/mm)^2$	Both, $(mm/mm)^2$	
0, no model	...	...	387.9	120,107.		
Decrease weight of two-color data by 5	...	...	...	4,804.3	5,192.2	
I, displacement at CASA (14a) and ellipsoidal point at 7.0 km	7.9	7.4	167.9	66.2	234.1	2.360
II, add dike under Mammoth (15a) Mountain, 2–12 km	7.8	7.2	130.0	78.9	208.8	...
III, add faulting in (16a) Smokey Bear Flat, 0–5 km	6.2	7.6	93.6	75.0	168.6	2.236
Comparison to Mogi [1958] Source Model						
IIIa, displacement at CASA and Mogi point at 11.5 km	...	...	90.8			
IIIb, displacement at CASA and Mogi point at 8.5 km	1.0	0.3	...	108.2		
IIIc, displacement at CASA and Mogi point at 10.5 km	−0.5	16.0	146.0	115.4	261.4	
Add IV, second ellipsoidal source (13a) $D = 13.0$	4.5	7.8	78.6	19.8	98.5	1.471
OR						
Dipping dike (10a), 10–14 km	4.9	4.5	77.1	37.9	115.0	1.771

Using 40 baselines and 106 sections.

The proximity of the common station CASA (Figure 1) to the localized subsidence associated with water withdrawal and heat extraction at the Casa Diablo geothermal field [*Sorey et al.*, this issue] means that line lengths measured by the two-color geodimeter may be contaminated. The location of the power plant is 1.1 km west of the station CASA and the width of the subsidence is approximately 2 km as shown by leveling along Route 395 in Figure 2c. Several strategies could be employed to model both the short-wavelength deformation of the geothermal field and the long-wavelength deformation due to inflation of the caldera. However, because of the lack of a unique model for the subsidence of the geothermal field we let the horizontal vector displacement of CASA be a free parameter in our search for optimal models describing the long-wavelength deformation. We remove from consideration those baselines and leveling sections that are highly influenced by the geothermal field including the 18 sections of leveling spanning the geothermal field and the baseline CASA-Numike (Figure 1). We then search for optimal models that satisfy the remaining 40 baselines and 106 sections for which the optimal models include an estimate of the displacement of CASA. Displacements of CASA obtained in our analysis (Table 2) show a range from 0 to 10 mm.

To test whether a range of 0- to 10-mm horizontal displacements of CASA is attributable to subsidence of the nearby geothermal field, we have constructed two models of the subsidence, one that predicts less than 1-mm displacement at CASA and a second that predicts 10-mm horizontal displacement. Both models involve the collapse of a flat-lying tensile fracture at 200 m depth. By partitioning the 1.5×3.0 km^2 plane into 72 smaller units, we used the near-field leveling and two geodimeter baselines, CASA to Numike and jcm, to map the collapse of the fracture. Because the number of model elements exceeds the number of observations, some smoothing was obtained by constraining the collapse of each cell to be between 0 and 20 cm. Because leveling does not extend to CASA, we found that the collapse of the fracture near CASA was poorly resolved so that the horizontal displacement of CASA from the subsidence of the geothermal field could easily range between 0 and 10 mm.

To model the long-wavelength deformation of the caldera, we employed the ellipsoidal point source model of *Davis* [1986] rather than the conventional *Mogi* [1958] point source, because the latter could not adequately fit both the uplift and horizontal line length changes. The Mogi model represents an increase in the radius of a spherical magma chamber at depth. Because surface measurements of deformation are not sensitive to the absolute radius of the source [*McTigue*, 1987], a point source approximation works well. The ellipsoidal point source is composed of three orthogonal double forces having unequal magnitude. The inversion of the data results in the six components of a stress tensor such that a suitable rotation can be applied to obtain the orientation of the principal axes and their strengths. The progression from a single source to more complex models to explain the observations is outlined in Table 2.

We start by fitting an ellipsoidal point source, termed model I, to a combination of leveling and two-color geodimeter measurements. Although this source at 7.0 km beneath the resurgent dome explains approximately 95% of the variance in the data, we find that significant signals remain. In particular, at 13 km along the Route 203 leveling (Figure 2b), there is an inflection that could be due to dike intrusion beneath Mammoth Mountain [*Hill et al.*, 1990]. In addition, short-wavelength fluctuations at the 28-km point along the Route 395 traverse and at the west end of the "small loop" shown in Figures 2a and 2b suggest displacement on a normal fault in Smokey Bear Flat. Adding dike intrusion (model II) and normal slip in Smokey Bear Flat (model III) significantly reduces the size of the residuals in the leveling data but slightly increases the residuals in the two-color data.

The most prominent feature of the deformation field is inflation of the resurgent dome, which we have modeled because of an ellipsoidal point source at a depth of 7.0 km. The location of this source is within 0.5 km of the point labeled "inflation" in Figure 1. The depth of 7.0 km provides an optimal fit to a combination of leveling and two-color data. The principal components of the stress tensor representing the inflation source are

$$P_1 = 13.6 \pm 0.3 \times \frac{\mu}{V}\ \text{MPa} \quad N(4 \pm 34)°E\ \text{down}\ (3 \pm 3)°$$

$$P_2 = 12.9 \pm 0.3 \times \frac{\mu}{V}\ \text{MPa} \quad N(87 \pm 34)°W\ \text{up}\ (6 \pm 5)°$$

$$P_3 = 10.1 \pm 0.2 \times \frac{\mu}{V}\ \text{MPa} \quad N(59 \pm 11)°W\ \text{up}\ (84 \pm 2)°$$

where the first angle is the azimuth of the principal axis and the second is the angle with respect to the horizontal. The value μ is the shear modulus, and V is the total volume of the source, which must be estimated from other data.

A dike intrusion beneath Mammoth Mountain, which has been postulated by *Hill et al.* [1990] as the cause of a swarm of earthquakes during mid-1989, can be modeled from the leveling data. The optimal model, consisting of a rectangular, vertical dike between 2 and 12 km depth, provides a satisfactory fit to the data (Figure 2b, Route 203). Even though there are two-color geodimeter measurements to the south of Mammoth Mountain [*Langbein et al.*, 1993a], these measurements do not span the 1988–1992 interval discussed here, and therefore they are not used for modeling. Instead, for the Mammoth Mountain area we use the results of modeling the geodimeter measurements south of Mammoth Mountain by *Langbein et al.* [1993a] to constrain the southwest edge of the modeled dike. The results of the modeling here suggest that the dike opened by 134 ± 21 mm during the 1988–1992 interval.

In addition to dike intrusion the leveling data suggest that at least one of the normal faults of the medial graben in the central caldera was activated. By using the grid search technique and the locations of surface faulting provided by the geologic map of *Bailey* [1989], we found that 54 ± 8 mm of slip on a fault in Smokey Bear Flat near Route 395 fit the leveling data. This modeled fault extends from the surface to a depth of 5 km and dips 65° to the east. The fault parameters of dip and width are poorly constrained.

From the value of misfits χ^2 from model III, it is apparent that there remains significant signal in the two-color data. Whereas χ^2 for leveling of 91.6 $(\text{mm/mm})^2$ is less than the number of sections, indicating a satisfactory fit of the model to the leveling data, the value of $\chi^2 = 67.9\ (\text{mm/mm})^2$ for the two-color data exceeds the number of baselines of 40.

The results of modeling either dike intrusion or a second ellipsoidal source beneath the caldera are shown in Table 2 and Figure 1. Both models imply a source of intrusion beneath the south moat of the caldera. The ellipsoidal source provides a significantly better fit to the two-color data than does the dike. When either the second ellipsoidal source or the dike under the south moat is included, the optimal solution indicates that the inflation source beneath the resurgent dome becomes slightly shallower, 5.5 km rather than the 7.0 km estimated previously. For the model that best fits the data we find that the 5.5 km source beneath the resurgent dome has principal stress tensor components as

$$P_1 = 6.40 \pm 0.23 \times \frac{\mu}{V}\ \text{MPa} \quad N(32 \pm 30)°E\ \text{down}\ (5 \pm 3)°$$

$$P_2 = 6.03 \pm 0.33 \times \frac{\mu}{V}\ \text{MPa} \quad N(59 \pm 30)°W\ \text{down}\ (5 \pm 6)°$$

$$P_3 = 4.30 \pm 0.27 \times \frac{\mu}{V}\ \text{MPa} \quad N(11 \pm 13)°W\ \text{up}\ (83 \pm 3)°$$

The principal stress tensor components for the source located 13 km below the south moat are

$$P_1 = 16.3 \pm 2.3 \times \frac{\mu}{V}\ \text{MPa} \quad N(7 \pm 43)°E\ \text{up}\ (22 \pm 21)°$$

$$P_2 = 13.3 \pm 1.7 \times \frac{\mu}{V}\ \text{MPa} \quad N(70 \pm 33)°W\ \text{down}\ (29 \pm 31)°$$

$$P_3 = 4.6 \pm 1.0 \times \frac{\mu}{V}\ \text{MPa} \quad N(65 \pm 14)°E\ \text{down}\ (52 \pm 9)°$$

We can use the ratio of the principal stresses to obtain the ratio of lengths of the ellipsoidal axes from *Davis* [1986], but we cannot obtain the total volume of the ellipsoidal inclusion on the basis of geodetic data alone. Using Table 1 of *Davis* [1986], we find that for the inflation source beneath the resurgent dome the ratios in axis lengths are $l_1/l_3 = 0.25$ and $l_2/l_3 = 0.24$. For the source beneath the south moat the ratios in axis lengths are $l_1/l_3 \approx 0$ and $l_2/l_3 \approx 0$. Thus the source beneath the resurgent dome has a vertical axis that is about 4 times longer than its two horizontal axes, and the south moat source is an elongated ellipse or pipelike structure that dips 52° in a N65°E direction.

To show that the models constructed using the leveling data and the temporally decimated two-color data are consistent with all of the two-color measurements, we constructed a time-dependent function of each source using the method of *Langbein* [1989] and evaluated the misfit of the model to the observations. For models I, III, and IV the value of the normalized RMS misfit is tabulated in Table 2. To reduce the number of time-dependent terms with the ellipsoidal sources, we combine the six components of the stress tensor into a single scalar by assuming that the ellipsoidal source has a constant geometry in time. That is, the ratio between the components of the stress tensor remain invariant. Examination of the misfit ratio shows that the successive improvements achieved from model I to model IV constructed using both the leveling and decimated two-color data are reflected in better fits to all of the two-color data. We consider the misfit ratio of less than 1.5 with model IV to indicate a satisfactory fit of the model with the two-color measurements since the time-dependent error associated with potential monument noise has not been factored into the a priori error of the two-color measurements.

Sensitivity Analysis

To examine the individual contributions of leveling and two-color data estimating the location of the inflation beneath the resurgent dome, we use the simple *Mogi* [1958] point source since this model of uniform pressure change could adequately satisfy each data set separately (Table 2, models IIIa and IIIb). The results of the sensitivity analysis for each data set is shown in Figure 3, where the summation of the misfit χ^2 is plotted against different trials in position and depth of a point source. The residuals in the two-color data are very sensitive to the source position. By using the F test we can demonstrate that source models having depths of

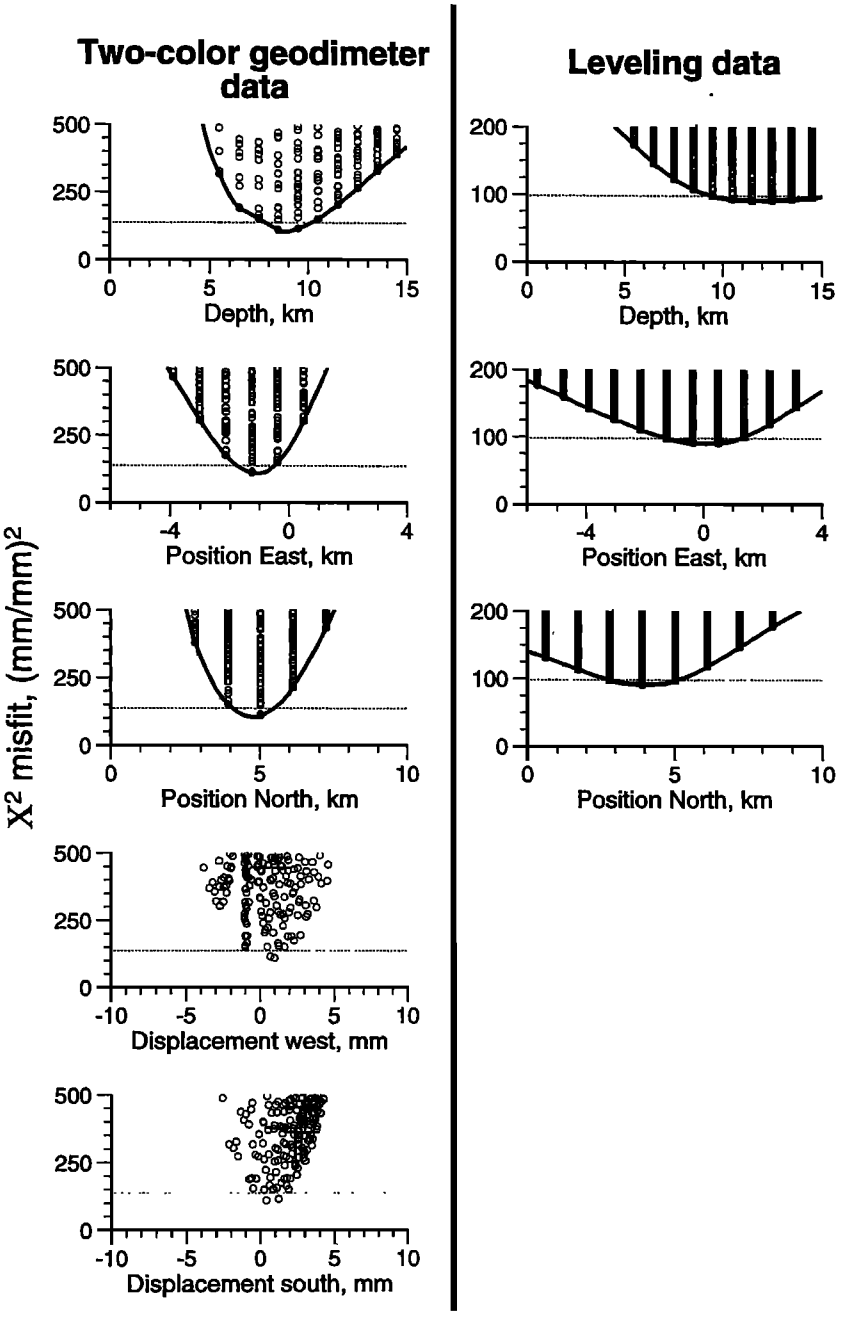

Figure 3. Sensitivity of the misfits to the data of a *Mogi* [1958] point source model using different locations and depths relative to station CASA (37.6444 and 118.8956). (left) The sensitivity of the two-color data to different source locations and the range in inferred displacement of CASA. (right) The sensitivity of the leveling data to different source locations. Each small cross represents the value of χ^2 for a specified location. A grid search algorithm was used to obtain the optimal solution. No optimal solutions could be found beneath the solid curved lines. The dashed horizontal line shows the increase in the value of χ^2 needed to reject the models at the 95% confidence level using the F test.

less than 7 km or greater than 11 km can be rejected at the 95% confidence level. A change in horizontal position of less than 1 km on either side of the optimal location can also be rejected at the 95% confidence level. The leveling data are slightly less sensitive to the position of the source than the two-color data. For instance, a change in the horizontal position of the point source by 1.5 km on either side of the optimal location can be rejected at the 95% level, and the depths of less than 9 km or greater than 15 km can be rejected at the 95% confidence level.

The poor fit of the Mogi model to both the leveling and the two-color data is demonstrated in Table 2 and is listed as model IIIc. We used the same constituents as model III with the displacement of CASA being treated as an unknown plus dike injection beneath Mammoth Mountain and normal faulting in Smokey Bear Flat. For a prescribed source depth

the two-color data yield an estimated volume change that is between 50 and 100% more than the volume change estimated by leveling alone. Thus the Mogi model cannot satisfy the combined data set adequately.

When both data sets are used to estimate the parameters of an ellipsoidal source (model III), we find through sensitivity analysis that the optimal depth lies within 1 km of 7 km (95% confidence level) and the horizontal position lies within 0.8 km of the optimal location (again, 95% confidence level).

The sensitivity of the data to the position of the second source indicates that its depth lies between 10 and 20 km and its horizontal position can range asymmetrically on either side of the optimal location before the models can be rejected at the 95% confidence levels. That is, an acceptable location could range from 3 km north to 5 km south of the optimal location and from 2 km east to 6 km west of the optimal location shown in Figure 1.

Discussion

Our results indicate that the source of inflation beneath the resurgent dome is shallower than estimated in previous analyses of Long Valley deformation data. Although poorly resolved, we find that a second, deeper source is active beneath the south moat or the Sierran block just south of the caldera. The apparent decrease in depth of the modeled source beneath the resurgent dome is due to the inclusion of the second source of inflation. If the data are modeled with only a single source of inflation (model III), its optimal depth is 7 km, consistent with the previous analyses [*Langbein et al.*, 1993a]. As in the previous study by *Langbein et al.* [1993a], we also had unacceptably large misfits of our model III involving a single source with the line length changes measured on some baselines. In the previous study the misfits of the model were reduced by incorporating normal slip on one of the medial graben faults near stations RODGER and TUP. That model predicts an approximately 5-cm offset at the 10 km point of the Little Antelope Valley leveling traverse (Figures 1 and 2), but no such offset was detected near this point (Figure 2b). Therefore, to satisfy both the two-color geodimeter data and the leveling data, we needed another source rather than slip on the medial graben. The model with either a dike or a pipe located at >10 km depth beneath the southern part of the caldera satisfies the data with our preferred interpretation being an inflation of a pipe which is represented by an ellipsoidal source with a single, long axis.

The existence of the second source of inflation also is consistent with annual Global Positioning System (GPS) measurements made near and within the caldera. M. Lisowski and M. Murray (personal communication, 1994) have modeled these measurements using *Mogi* [1958] point sources and found that the addition of a second source south of the caldera achieved a better fit than the single source beneath the resurgent dome. We have tested model IV on GPS data and found that the predicted displacements are also consistent with the GPS data.

Recent interpretations of seismic data by *Ponko and Sanders* [1994] and *Steck and Prothero* [1994] show evidence of possible magma chambers, and the inferred locations of these chambers are adjacent to the currently active sources of inflation found geodetically. *Ponko and Sanders'* [1994] interpretation of *S* wave attenuation suggests that the top of the magma chamber is 7–8 km beneath the southern margin of the resurgent dome and adjacent to our 5.5-km-deep source. Whereas Ponko and Sanders used local earthquake data to examine the shallow structure, *Steck and Prothero* [1994] used teleseismic data to examine the deeper structure of the crust. Their study shows large, low-velocity volume between 7 and 11 km extending over an 8-km-wide area from Mammoth Mountain and the center of the resurgent dome which is roughly similar to the volume mapped by *Ponko and Sanders* [1994]. Neither seismic study, however, resolves anomalies in crustal structure that correspond to the sources of active inflation that have been described here. Rather, our sources seem adjacent to those found seismically.

The existence of dike intrusion beneath Mammoth Mountain in mid-1989 that had been hypothesized by both *Hill et al.* [1990] and *Langbein et al.* [1993a] is supported by the leveling data along Route 203 presented here. Even though the location of earthquake epicenters beneath Mammoth Mountain implies that the dike intrusion may be centered at 6–9 km depth, the modeling of geodetic data presented here and by *Langbein et al.* [1993a] indicates that the intrusion was actually much shallower. By using the *F* test with a 95% confidence level we find that acceptable models place the top of the intrusion ranges between 1 and 3 km depth.

Finally, examination of the time dependence constructed from model IV is similar to that discussed by *Langbein et al.* [1993a]. That is, the inflation source beneath the resurgent dome shows a sudden increase in rate starting in late 1989. This rate decreased about 50% in March 1990 but has been steady since then [*Langbein et al.*, 1993a, Figure 10]. The temporal correlation is low between the auxiliary 6.5-km source identified by *Langbein et al.* [1993a] and the 13-km-deep source proposed here. The previous result showed that this source was nearly inactive during this second episode of inflation, but our results show that the 13-km-deep source is active.

The possible existence of intrusion deep beneath either the south moat or within the Sierran block south of the caldera is particularly interesting in that this source may provide the mechanical explanation between the high rate of seismicity both within the Sierran block south of the caldera and in the south moat. However, better constraints on the size, geometry, and location of the deep source will be difficult because of its proximity to the resurgent dome, and the strong signal contributed by the inflation of the resurgent dome obscures the surface deformation due to the deep source. Only with additional geodetic coverage south of the caldera, will we be able to better constrain the existence of the deeper source and understand its link with the mechanics of the caldera.

Conclusions

Our inferences from the combination of leveling and trilateration show that the hazard persists owing to intrusion of magma beneath the Long Valley caldera. The current network of line length measurements using the two-color geodimeter is very sensitive to any changes in inflation rate that may occur in the postulated magma source beneath the resurgent dome. Periodic leveling data are important for determining the geometry of the sources and identifying the Mammoth Mountain intrusion but do not provide the critical temporal information needed to assess the potential hazard posed by magma beneath the resurgent dome. The best

temporal information of deformation from geodesy comes from the frequent measurements, made several times per week, of the baselines using CASA with the two-color geodimeter.

With the current baselines within the two-color geodimeter network we have only minimal coverage near Mammoth Mountain should another episode of intrusion occur there. Following the earthquake swarm beneath Mammoth Mountain in 1989, *Langbein et al.* [1993a] established additional baselines near the postulated intrusion, but as demonstrated by *Langbein et al.* [1993a], the data from these baselines provide minimal constraints on the geometry of intrusion. It is the leveling data discussed here that provide more convincing evidence of intrusion beneath Mammoth Mountain.

Acknowledgments. Careful reviews by Paul Davis, Jim Savage, and Dave Hill improved this manuscript. This research was supported in part under the auspices of the U.S. Department of Energy by contract W-7405-ENG-48 to Lawrence Livermore National Laboratory.

References

Arnadottir, T., P. Segall, and M. Matthews, Resolving the discrepancy between geodetic and seismic fault models for the 1989 Loma Prieta, California, earthquake, *Bull. Seismol. Soc. Am.*, *82*, 2248–2255, 1992.

Bailey, R. A., Geologic map of the Long Valley caldera, Mono-Inyo Craters volcanic chain, and vicinity eastern California, *U.S. Geol. Surv. Misc. Invest. Map*, *I-1933*, 2 sheets, 11 pp., 1989.

Davis, P. M., Surface deformation due to inflation of an arbitrarily oriented triaxial ellipsoidal cavity in an elastic half-space, with reference to Kilauea Volcano, Hawaii, *J. Geophys. Res.*, *91*, 7429–7438, 1986.

Dixon, T., M. Bursik, S. Wolf, M. Heflin, F. Webb, F. Farina, and S. Robaudo, Constraints on deformation of the resurgent dome, Long Valley caldera, California from space geodesy, in *Contributions of Space Geodesy to Geodynamics: Crustal Dynamics*, *Geodyn. Ser.*, vol. 23, edited by D. E. Smith and D. L. Turcotte, pp. 193–214, AGU, Washington, D. C., 1993.

Hill, D. P., W. L. Ellsworth, M. J. S. Johnston, J. O. Langbein, D. H. Oppenheimer, A. M. Pitt, P. A. Reasenberg, M. L. Sorey, and S. R. McNutt, The 1989 earthquake swarm beneath Mammoth Mountain, California: An initial look at the 4 May through 30 September activity, *Bull. Seismol. Soc. Am.*, *80*, 325–339, 1990.

Langbein, J., Deformation of the Long Valley caldera, eastern California, from mid-1983 to mid-1988: Measurements using a two-color geodimeter, *J. Geophys. Res.*, *94*, 3833–3850, 1989.

Langbein, J., M. Linker, and D. Tupper, Analysis of two-color geodimeter measurements of deformation within the Long Valley caldera: June 1983 to October 1985, *J. Geophys. Res.*, *92*, 9423–9442, 1987.

Langbein, J. O., D. P. Hill, T. N. Parker, and S. K. Wilkinson, An episode of reinflation of the Long Valley caldera, eastern California: 1989–1991, *J. Geophys. Res.*, *98*, 15,851–15,870, 1993a.

Langbein, J., E. Quilty, and K. Breckinridge, Sensitivity of crustal deformation instruments to changes in secular rate, *Geophys. Res. Lett.*, *20*, 85–88, 1993b.

McTigue, D. F., Elastic stress and deformation near a finite spherical magma body: Resolution of the point source paradox, *J. Geophys. Res.*, *92*, 12,931–12,940, 1987.

Mogi, K., Relations between eruptions of various volcanos and the deformation of the ground surface around them, *Bull. Earthquake Res. Inst. Univ. Tokyo*, *36*, 99–134, 1958.

Ponko, S. C., and C. O. Sanders, Inversion for *P* and *S* wave attenuation structure, Long Valley caldera, California, *J. Geophys. Res.*, *99*, 2619–2635, 1994.

Rundle, J. B., and J. H. Whitcomb, Modeling gravity and trilateration data in Long Valley, California, *J. Geophys. Res.*, *91*, 12,675–12,682, 1986.

Savage, J. C., Principal component analysis of geodetically measured deformation in the Long Valley caldera, eastern California, *J. Geophys. Res.*, *93*, 13,297–13,306, 1988.

Sorey, M. L., C. D. Farrar, G. A. Marshall, and J. F. Howle, Effects of geothermal development on deformation in the Long Valley caldera, eastern California, 1985–1994, *J. Geophys. Res.*, this issue.

Steck, L. K., and W. A. Prothero, Crustal structure beneath Long Valley caldera from modeling of teleseismic *P* wave polarizations and *Ps* converted wave, *J. Geophys. Res.*, *99*, 6881–6898, 1994.

Wyatt, F., Displacements of surface monuments, *J. Geophys. Res.*, *87*, 979–989, 1982.

Yamashita, K. M., J. W. Kleinman, E. Y. Iwatsubo, J. W. Ewart, D. Dzurisin, J. B. Rundle, and R. S. Stein, Results of 1992 leveling survey at Long Valley caldera, California, *Eos Trans. AGU*, *73*(43), Fall Meet. suppl., 347, 1992.

D. Dzurisin, U.S. Geological Survey, 5400 MacArthur Blvd., Vancouver, WA 98661. (e-mail: dzurisin@pwavan.wr.usgs.gov)

J. Langbein, G. Marshall, and R. Stein, U.S. Geological Survey, 345 Middlefield Road, MS 977, Menlo Park, CA 94025. (e-mail: langbein@shasta.wr.usgs.gov; gmarshall@isdmnl.wr.usgs.gov; rstein@isdmn1.wr.usgs.gov)

J. Rundle, Cooperative Institute for Research in Environmental Science, University of Colorado, Boulder, CO 80309. (e-mail: rundle@fractal.colorado.edu)

(Received September 1, 1994; revised February 15, 1995; accepted March 28, 1995.)